

Experimental Study of Oil Flow Visualization on the Analysis on Airfoil Eppler 562 of the Use of Forward and Rearward Wingtip Fences 75o Cant Angle Article

Bayu Dwi Cahyo*, Gunawan Sakti, Ajeng Wulansari, Bambang Junipitoyo

Politeknik Penerbangan Surabaya, Jemur Andayani 1/73 Wonocolo Surabaya, Jawa Timur, Indonesia, 60236

*Corresponding Author. Email: bayu_dwi@poltekbangsby.ac.id

ABSTRACT

In this study, the flow over airfoil Eppler 562 with and without wingtip was investigated experimentally. The experiments were carried out in a low speed wind tunnel with various angles of attack (α) = 0° to 19°. The Reynolds (Re) number used is 2.3×10^4 ($U^\infty = 10$ m/s). There are two types of wingtip fences at variations that will be used in this research that are rearward and forward wing tip fence set at cant angle 75°. For this research, to represent flow patterns on airfoil the Oil flow visualization method was used. pressure transducer used to measure pressure distributions over the airfoil. The experimental results showed that as the angle of attack increased, the transition points and the separation moved towards the leading edge at all models. Furthermore, for airfoil with forward wingtip fence with cant angle 75° is better than for airfoil with rearward wingtip fence with cant angle 75° and plain wing. Forward wingtip fence showed the best optimum performance of $\alpha = 10^\circ$ settings compared to the other models. Consequently, it was seen that there was a good agreement between numerical and experimental results.

Keywords: Eppler 562, wingtip fence, cant angle, induced drag reduction, oil flow visualization,

1. INTRODUCTION

Many studies in recent years have aimed at improving the aerodynamic performance of a wide range of aircraft have been growing rapidly and promisingly. Due to the limited length of the wing, the pressure difference above and below the airfoil creates a three-dimensional flow at the tip that called vortex. vortex is circular pattern of air flows from lower the wing to the upper of the wing around the wingtip This flow created a vortex, the so-called tip vortex. The tip vortex creates separation and vortices that increase the drag component and reduce lift, thereby reducing the effectiveness of the wingspan. These vortexes can also cause several problems for aircraft during flight activities, including excessive fuel consumption due to the large drag force and noise produced by the vortex. The airfoil shape and its modifications are the important point to consider when designing an aircraft. The advantages of optimal design are reduced drag and increased lift. One attempt to reduce the vortex is delaying the separation. Another attempt is wingtip modifications by addition of winglet.

The numerical simulation the wing design and winglet variants were studied at different bank angles (0°, 30° and 90°) and attack angles (-2° to 10°). In this study, it was found that winglets improve the CL/CD ratio of the airfoil [2] [7]. The studies to analyze aerodynamic performance of wingtip fences at various cant angles on airfoils in the form of forward and rearward wingtip fences, increasing CL/CD value up to 22. 9% for forward wingtip fence at $\alpha = 2^\circ$ [4].

Wing with E420 airfoil, at a speed of 10 m/s or $Re = 10^5 - 3 \times 10^5$. With low angle of attack, plain wing has higher lift coefficient than wing blended winglet. At $\alpha = 7^\circ$, wing blended winglet has higher lift coefficient until stall point. In the study, winglets were found to reduce drag coefficient at all angles of attack. Results indicate constant induced drag but decreasing lift friction drag [5].

In a study by Dr. Basawaraj et al. A computational analysis was done on the NACA-65(3)-218 wing to decrease lift-induced drag force, which makes up 30-40% of the wing's total drag force. The results showed that the Rake and L-winglet are more effective than the clean winglet at higher angles of attack. Rake winglets outperform clean winglets at an 8° angle of attack with a

high L/D ratio of 8. L – Winglet performs even better than clean and Rake winglets at an 8° angle of attack with a high L/D ratio of 10. However, all three wing configurations perform worse as the angle of attack increases from 8° to 16° [1].

This study used an Eppler 562 (E562) airfoil without and with the addition of a wingtip fence to evaluate aerodynamic performance. There are two types of wingtip fence variations that will be used in this study to see the effect of wingtip fences in increasing wing performance and reducing drag occurring at certain angles of attack.

2. RESEARCH METHODOLOGY

2.1 Models and Wind Tunnel

The airfoil models were manufactured out of acrylic sheet (Figure 1) that was formed according to airfoil Eppler 562 profile. The manufactured airfoils have a span length of 0.3 m, and a chord length of $c = 0.072$ m. the profile winglet maximum chord forward wingtip fence from leading edge and winglet maximum chord rearward wingtip fence from leading edge are 0.072 m and 0.022 m respectively, and the winglet minimum chord is 0.015 mm (Figure 2).

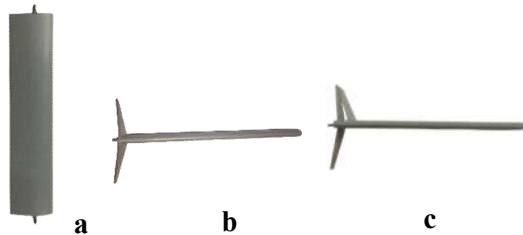


Figure 1 Airfoil models manufactured: a) plain wing b) forward wingtip fence cant angle 75° and c) rearward wingtip fence cant angle 75° .

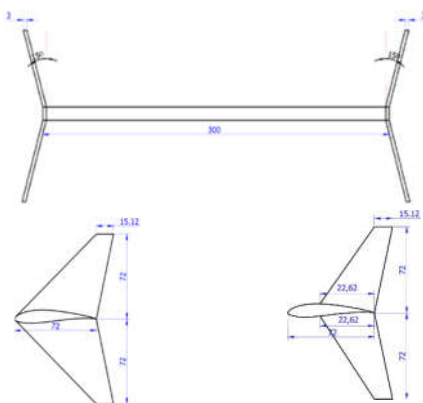


Figure 2 Dimension airfoil models: a) side-view forward wingtip fence cant angle 75° and c) side-view rearward wingtip fence cant angle 75°

2.2 Wind Tunnel Set-Up

The experiments were carried out at the aerodynamics laboratory of the Aeronautical Polytechnic University in Surabaya. The experiments took place in a low-speed suction wind tunnel with a test cross-section of 600 mm x 600 mm. The area ratio of the contraction cone is $\pm 9:1$ and the side walls of the work area have a divergence angle of zero. To minimize boundary layer effects and maintain constant static pressure, the walls of the work area must be shortened to 3° each side. The blower can reach a maximum air speed of 50 m/s. Experiments were conducted at Re number 2.3×10^4 using airfoil string length (c) and free stream velocity (U_∞). Figure 1 and Figure 3 show the Wind tunnel set-up.

The blockage effect on the experimental results is negligible when the intercept is less than 10% [9] [11]. The blockage ratio wind tunnel of the Eppler 562 at 0° angle of attack in our wind tunnel is $0.3 \times 0.15 \times 0.72 / (0.6 \times 0.6) = 0.009$ ($\sim 0.9\%$). The blockage ratio wind tunnel of the Eppler 562 at a 19° angle of attack is 0.018 ($\sim 1.8\%$).



Figure 3 Wind tunnel set-up

2.3 Pressure Measurements

A system was used to measure pressure distributions on the Eppler 562 airfoil. It included a pitot-static tube, a National Instrument unit, a 32-channel pressure transducer, and 32 pressure tapping of 1/16 inch in diameter. The tapping was flush along the mid-span and tip-span alternately of the upper and lower surfaces of the wing (Figure 4). Pressure was measured using a computer data acquisition system, specifically the ni cdaq-9172 National Instrument, which provided a voltage output. The pressure transducer had a maximum response time of 1 ms. Pressure signals were obtained at a sampling rate of 100 samples per second using Signal Express software. The software converted the analog pressure data to digital (A/D) in ASCII format. Datapost-processing was performed in Microsoft Excel software to calculate mean pressure distributions and create a graph. Experiments examined various angles of attack to determine pressure coefficient distribution on airfoils.



Figure 4 Pressure tap location on mid span and tip span at all models.

2.3 Oil Flow Visualization

To observe surface flow events, we visualize oil flow on a matte black airfoil surface (**Figure 5**). We paint the surface before applying colored oil during wind tunnel experiments. The oil mixture must match the blower's speed and consistency to indicate boundary layer development effectively. The moving oil's inertial force should be smaller than surface tension and viscous forces to avoid affecting surface conditions. The recommended mixture is palm oil and titanium dioxide (TiO₂), with a ratio of 5:1. Stir for 15 minutes until TiO₂ particles are no longer visible. This mixture is diluted with kerosene in a 5:1 ratio [9] [10]. This mixing ratio was used in the study, but colorants are dosed based on Reynolds number.

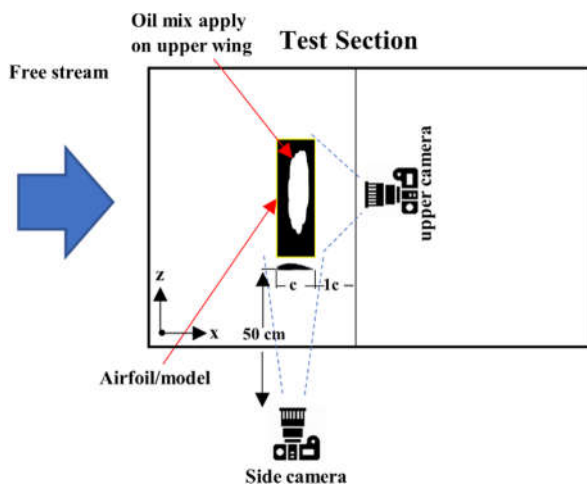


Figure 5 Schematic diagram of the experimental oil flow visualization set-up.

3. RESULTS AND DISCUSSION

In **Figure 6**, a visualization of the flow pattern on the upper side of the plain wing type Eppler 562 airfoil with an angle of attack (α) of 0°, 4°, 8°, and 12° is shown. Oil flow visualization is used to understand the concepts of laminar flow, laminar separation bubble, separation and turbulent flow that occur in the airfoil. In general, oil flow visualization will provide information that there is no change in the density of the oil mixture above the airfoil resulting in flow separation or separation.

Meanwhile, the oil mixture will be swept away at the flow location attached to the surface due to the influence of viscous and pressure gradients on the airfoil.

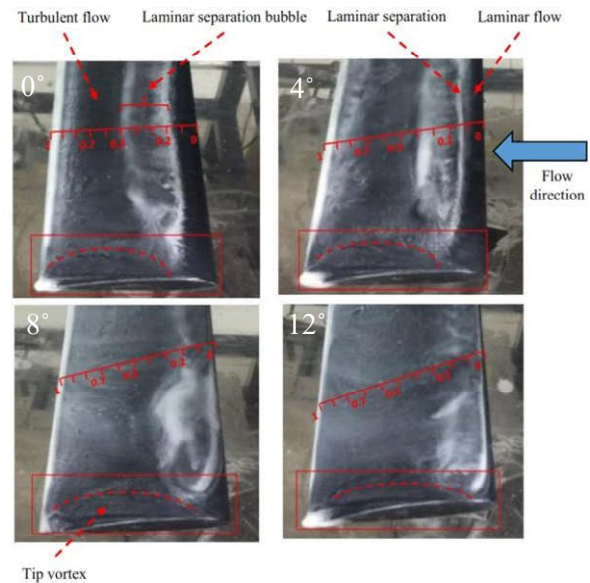


Figure 6 The photographs of oil-flow visualization experiments over the Eppler 562 airfoil plain wing at angle of attack (α) 0°, 4°, 8° and 12° on $Re = 2.3 \times 10^4$

In general, in **Figure 6** with different angles of attack, when the angle of attack increases it will be followed by a change in the separation point which is increasingly approaching the leading edge [3]. On the wing tip, it can be seen that there is an area with a low oil mixture density. This is caused by a flow leak from the lower side to the upper side creating a tip vortex which has a higher speed sweeping the oil mixture at the wingtip towards the span (spanwise flow). This flow will rotate towards the center of the wing, marked by some of the oil mixture being swept towards the center of the wing.

It can be seen that the higher the angle of attack, the more pigmented area swept up on the wing tip extends towards the leading edge of the wing tip and it is possible that flow leakage has reached the leading edge. This flow leak starts from the trailing edge to the leading edge [3]. As a result of the leak at the leading edge, it is possible that there will be a decrease in pressure, which is indicated by the oil mixture being swept along the wing tip. This condition shows that the tip vortex formed is getting bigger. These vortices increase drag because their energy is used to create air turbulence. As a result, the effective area along the wing will decrease due to secondary flow, namely the flow separating the two boundary layers between the wing chord and the tip. It can be concluded that when the wing produces lift, induced drag and vortex will occur at the wingtip.

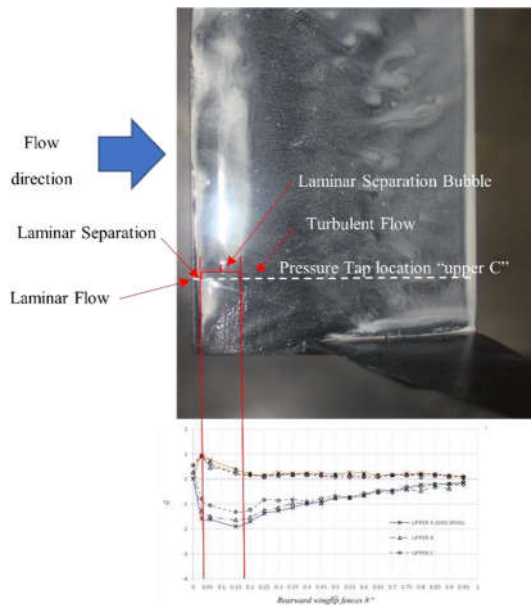


Figure 7 experiment result between oil-flow visualization vs Cp Distribution on airfoil Eppler 562 at (α) 8° , $Re = 2.3 \times 10^4$

Figure 7 shows the relationship between the quantitative results of the Cp distribution and the qualitative results of oil flow visualization at an angle of attack (α) of 12° where the pressure tap is placed on the wing tip (C: $c/s = 0.95$). In **Figure 7**, it is known that laminar flow conditions are characterized by a thin level of pigment density. This is because the flow velocity reaches a maximum value at the shoulder of the airfoil and has a negative pressure gradient so that it sweeps away almost all the oil mixture pigments. The laminar separation bubble condition is an area where the pressure gradient begins to decrease, almost reaching zero. On the Cp distribution graph, LSB is displayed by an area of constant pressure, which causes the Cp distribution curve to move gently. This condition is characterized by a high level of oil mixture pigment density. Then the Cp distribution curve recovers as a consequence of reattachment. As the angle of attack increases further, the separation point will move towards the leading edge. Furthermore, at a certain angle of attack the flow is no longer able to adhere to the airfoil surface for a short distance. This phenomenon is called breakdown or burst bubble.

The occurrence of this breakdown phenomenon does not cause the flow to separate completely. However, this flow will separate and flow over the surface of the airfoil and then reattach at a greater distance downstream. The existence of a slowly rotating flow region below the flow that is separated from the surface is called a dead-air region or long bubble. Then, the flow experiences massive separation due to the fluid's momentum being unable to resist the increasingly positive APG and the accumulation of shear stress that occurs. Behind the separation point, turbulent flow occurs where some of the

fluid experiencing back flow has a low pressure followed by an increase in speed marked by the washing away of the oil mixture.

On the **Figure 8** and **9**, it describes the concept of boundary layer separation, visualizing oil flow compare Cp distribution applied to the upper surface of an airfoil at angles of attack of 0° , 4° , 8° , and 12° . The pigment-dense region describes decelerating flow, that is, the point at which the fading pressure gradient causes separation. As the angle of attack increases, the separation point moves forward at all four angles of attack, and the magnitude of the vortex increases as the angle of attack increases. It shown the vortex formation at the tip where the plain wing creates the widest vortex contour. The front wingtip fence produces the smallest swirl contour compared to other types. Indeed, the formation of vortices at the fin tip is hindered by the fin tip. Therefore, the fairing design from the front to the rear end of the wing tip causes the air flow that tends from below near the wing tip to "jump" to the upper surface and can be effectively reduced. As the turbulence of the air flow from the lower surface is reduced, the area for vortex formation is reduced. This leads to an increase in lift coefficient.

The comparison of flow visualization on the upper side of the Eppler 562 plain wing airfoil and with the addition of rearward endplates and forward wingtip fence cant angle 75° , with angles of attack (α) 0° , 4° , 8° and 12° . In the wing tip section of the plain wing model and with the addition of the rearward wingtip fence, it can be seen that there are areas with low oil mixture density. This is because in both types of model there is a flow leak from the lower side to the upper side creating a tip vortex. This vortex tip has a higher speed which is able to sweep the oil mixture from the wingtip towards the span (spanwise flow). Then, this causes the flow to rotate towards the center of the wing, marked by some of the oil mixture being swept towards the center of the wing.

In **Figure 8** and **9**, it can also be seen in the plain wing model type and with the addition of a rearward wingtip fence, the higher the angle of attack, the pigmented area swept up on the wing tip expands towards the leading edge of the wingtip. Meanwhile, for the type of model with the addition of a forward wingtip fence, there is an area with a high oil mixture density at the wing tip. This is due to the absence of flow leakage from the lower side to the upper side which creates a tip vortex blocked by the endplate. This condition will improve wing performance because the effective span area on the wing tip will increase optimally compared to the other two types of models. From this information it can be concluded that the forward wingtip fence type is the most effective in improving wing performance in the tip region compared to the plain wing and rearward wingtip fence.

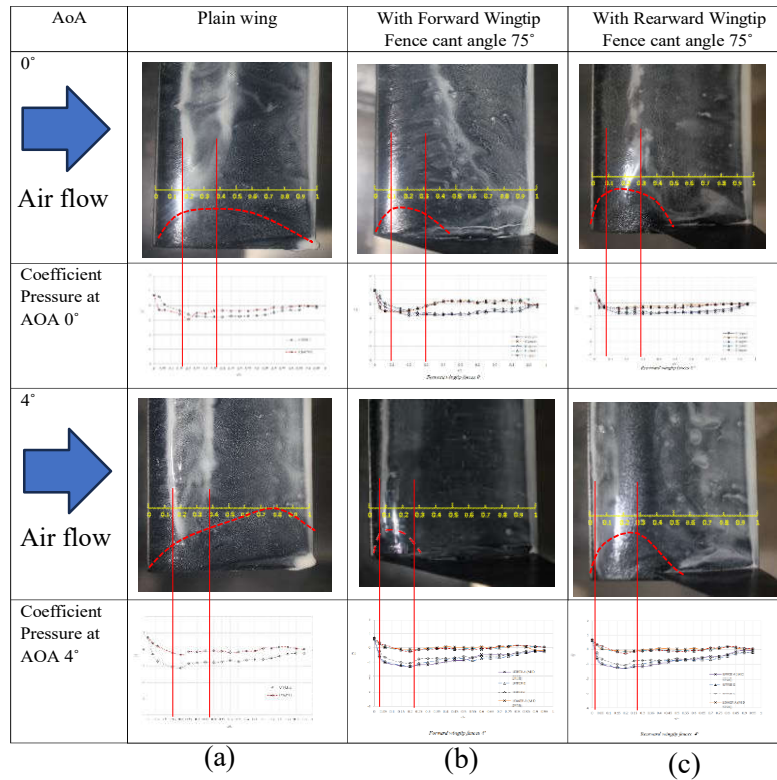


Figure 8 The photographs of oil-flow visualization vs Cp distributions experiments over the Eppler 562 airfoil for $\alpha = 0^\circ$ and 4° (a) plain wing (b) rearward wingtip fence (c) forward wingtip fence

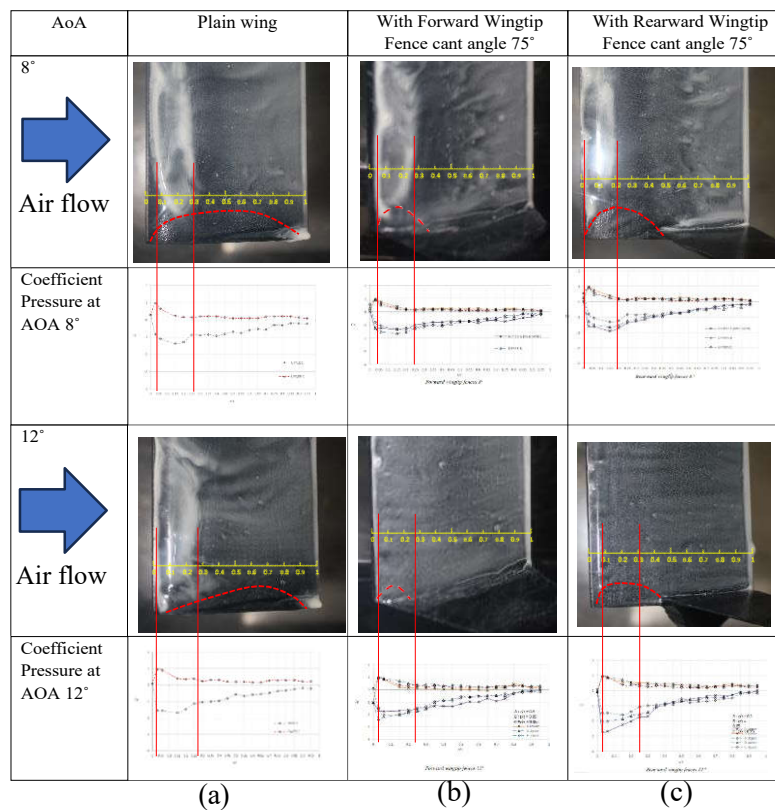


Figure 9. The photographs of oil-flow visualization vs Cp distributions experiments over the Eppler 562 airfoil for $\alpha = 8^\circ$ and 12° (a) plain wing (b) forward wingtip fence (c) rearward wingtip fence.

3. CONCLUSION

The results of this experimental investigation show that the use of winglets can improve the performance of the Eppler 562 airfoils. The use of variations in the wingtip fence increases drag as well as the angle of attack. However, with the addition of a winglet, lift can be improved better than with a single wing. Winglet significantly reduces the formation of swirl tips. Experimental research has concluded that the use of winglets can produce certain flow characteristics, namely:

- Wingtip vortices and drag coefficient will be increased as well as angle of attack increase.
- At begin Angle of Attack $\alpha = 6^\circ$ the best performance on forward wingtip fence cant angle 75° while at $\alpha = 8^\circ$ produce better performance for rearward wingtip fence cant angle 75°
- Forward wingtip fence cant angle produce smallest vortex formation area at tip than other types that performed by oil-flow visualization.
- The higher the angle of attack, the wider the vortex shape. As the vortex formation area increases, the lift coefficient decreases.

ACKNOWLEDGMENTS

This works was supported by Grant from Politeknik Penerbangan Surabaya due to sponsored this paper.

REFERENCES

- [1] Basawaraj, K. Prateekkumar R Kotegar, and Lokesh. M. H., CFD Simulations of Various Shapes of Winglets. International Journal: Visvesvaraya Institute Of Advanced Technology, 2016.
- [2] Demir, H., Özden, M., Genç, M. S., & Çagdas, M. , Numerical investigation of flow on NACA4412 aerofoil with different aspect ratios. In European Physical Journal Web of Conferences, 2016, (Vol. 114).
- [3] Genç MS, Karasu I and Açikel H , An experimental study on aerodynamics of NACA2415 aerofoil at low Re numbers, Experimental Thermal and Fluid Science, vol. 39, 2012, pp. 252–264.
- [4] Hariyadi S. P., Sutardi, and Wawan Aries Widodo, Drag reduction analysis of wing airfoil E562 with forward wingtip fence at cant angle variations of 75° and 90° , Proceedings of the 9th International Conference on Thermofluids (THERMOFLUID 2017), 2018, AIP Conf. Proc. 2001, 050003-1–050003-10. DOI: 10.1063/1.5049994
- [5] Kontogiannis, S. G., D. E. Mazarakos, and V. Kostopoulos. “ATLAS IV Wing Aerodynamic Design: From Conceptual Approach to Detailed Optimization.” Aerospace Science and Technology 56: 135–47, 2016, <https://doi.org/10.1016/j.ast.2016.07.002>.
- [6] Mehta. Anshuman, (2016), Different Types Of Winglets And Their Corresponding Vortices, 2016. Indian Institute of Technology,
- [7] Myilsamy D, Thirumalai Y and P SP, Performance Investigation of an Aircraft Wing at Various Cant Angle of Winglet Using CFD Simulation, in Altair Technology Conference, india, 2015
- [8] S.J. Schreck, N.N. Sorensen, M.C. Robinson (2007), Aerodynamic structures and processes in rotationally augmented flow fields, Wind Energy 10, 159–178.
- [9] Slavica R , Flow Visualisation Techniques in Wind Tunnels Part I – Non optical Method, Scientific Technical Review, vol. LVIII, no. 1, 2007
- [10] Sutrisno, Mirmanto H, Sasongko H and Noor DZ , “Study Of The Secondary Flow Structures Caused The Addition Forward Facing Step Turbulence Generated,” Advances and Applications in Fluid Mechanics, vol. 18, no. 1, 2015, pp. 129-144.
- [11] T.Y. Chen, L.R. Liou (2011), Blockage corrections in wind tunnel tests of small horizontal-axis wind turbines, Experimental Thermal and Fluid Science 35, 565–569.